Journal of Materials Science and Engineering B 11 (7-9) (2021) 89-96
doi: 10.17265/2161-6221/2021.7-9.001

Synthesis and Characterization of $Ni_{79}Fe_{15}Mo_6$ Nanoparticles Produced by Co-precipitation in the Presence of Organic Additives

Fabio Muchenski[1,2], Leonardo José Dalla Costa[3], Paulo Cesar de Camargo[3] and Ney Mattoso[2]

1. Instituto Federal Catarinense, São Bento do Sul, SC 89.283-064, Brazil

2. Departamento de Física da Universidade Federal do Paraná, Curitiba, PR 81.531-990, Brazil

3. Departamento de Física da Universidade Federal de São Carlos, São Carlos, SP 13.565-905, Brazil

Abstract: Stable nanoparticles of $Ni_{79}Fe_{15}Mo_6$ (at.%) were produced by co-precipitation by $NaBH_4$ in the presence of sucrose, ascorbic acid, and oleic acid. Nanoparticles are initially 3-10 nm in size and encapsulated by organic molecules. These particles clump together producing stable, spherical nanoparticles with an average diameter of 36 nm. Thermal analysis shows that from 600 °C no other mass loss process takes place. Preliminary magnetic measurements at room temperature show a typical behavior of a soft magnetic material, with a Mr of 1.41 emu/g (22% of Ms) and a Hc of 77 Oe. These results indicate that these nanoparticles produced by a simple, cheap, and ecologically friendly route, have a potential for diverse applications, but particularly for applications in the area of human and animal health.

Key words: Magnetic nanoparticles, supermalloy, co-precipitation.

1. Introduction

Since the appearance of the alloy, $Ni_{79}F_{16}eMo_5$ is also called Supermalloy by Boothby and Bozorth [1] in the form of massive materials. Over the past 20 years, several researchers have reported different ways to produce this Permalloy class magnetic alloy. Cowburn et al. [2] report the production of 2D supermalloy nanostructures through thin films produced by electron beam evaporation. Muñoz et al. [3] and Zhou et al. [4] report their success in producing thin films of supermalloy alloy by electrodeposition. The first works to synthesize micrometric particles of the Supermalloy alloy were reported by Chicinas et al. [5] and by Shen et al. [6], both using high-energy ball milling. With this same technique, several works were found [7-9]. The production of Supermalloy nanoparticles was reported by Musaev et al. [10] using laser ablation in water. It was also reported that Supermalloy alloy nanoparticles were produced by evaporation using the modified arc discharge method [11]. Only one work of the synthesis of NiFeMo nanoparticles was found, but outside the stoichiometry of the Supermalloy alloy, using a chemical route. Wang et al. [12] report success in synthesizing nanoparticles $Ni_{30}Fe_{20}Mo_{50}$ (at.%) by chemical co-precipitation using sodium borohydride ($NaBH_4$) as a reducing agent.

In the literature, it has been found the use of additives improves the characteristics of chemically synthesized nanoparticles, controlling morphological aspects such as size and shape, as well as stabilization and oxidation-reduction, in the case of transition metal particles [13]. For the development of this work, it was decided to use sucrose, ascorbic acid, and oleic acid as additives. The addition of sucrose in metal nanoparticle synthesis has been shown to be useful in controlling the mean size of Au nanoparticles [14] and as a protective layer against acid attacks on Ni nanoparticles [15]. The use of ascorbic acid in the

Corresponding author: Fabio Muchenski, Ph.D. student, professor, research fields: engineering and materials science.

green synthesis of metallic nanoparticles has been used as an encapsulation agent and consequent stabilization [13]. Alruqi et al. [16] reported the use of ascorbic acid as a reducing agent in Ag-Ni nanoparticles and as an inhibitor of the formation of Ni oxides and hydroxides during synthesis. Oleic acid has been reported in the literature as a stabilizing agent due to its affinity and due to the termination of the carboxylic acid which forms bonds with Fe atoms [17].

In this work, we are reporting our results in the synthesis of Supermalloy alloy nanoparticles by co-precipitation with the use of organic additives that make this synthesis route eco-friendly.

2. Experimental

NiFeMo nanoparticles were produced with reagent grade salts in 50 mL aqueous solution with 64 mmol of nickel chloride hexahydrate ($NiCl_2 \cdot 6H_2O$), 12.9 mmol of tetrahydrate iron chloride ($FeCl_2 \cdot 4H_2O$), and 1.63 mmol of sodium molybdate dihydrate ($Na_2MoO_4 \cdot 2H_2O$). A second 20 mL aqueous solution containing 2 mmol of sucrose ($C_{12}H_{22}O_{11}$), 1 mmol of ascorbic acid ($C_6H_8O_6$), and 2.535 mmol of oleic acid ($C_{18}H_{34}O_2$) was added as reagent grade organic additives. These solutions were mixed and a third 10 mL solution with sodium borohydride ($NaBH_4$) was dripped into the mixture under intense magnetic stirring at room temperature for 15 min. Then, the cleaning process was carried out by employing centrifugation. First, three wash cycles with double distilled water at 1,000 rpm were performed to separate most of the body from the bottom and excess oleic acid. Then, 10 cycles with isopropyl alcohol at 5,000 rpm were performed to remove any residue from the organic additives in the solution. At the end of the washing process, the supernatant nanoparticles were separated from the lower body and stored in isopropyl alcohol, as shown in Fig. 1.

For ex-situ characterizations, the following techniques were used. The TGA (thermogravimetric) and DTGA (differential thermogravimetric) analyses were performed on a Simultaneous Thermal Analyzer, model Netzsch STA 449 F3 Jupiter. Thermal measurements were performed with a heating ramp of 10 °C/min. in synthetic air (80% N_2, 20% O_2). The nanoparticles were placed in alumina crucibles for thermal analysis. Elementary chemical analysis by EDS (Energy Dispersive Spectroscopy) was performed with an 80 mm² SDD detector from Oxford coupled to SEM (Scanning Electron Microscopy) TESCAN, model VEGA3 LMU,

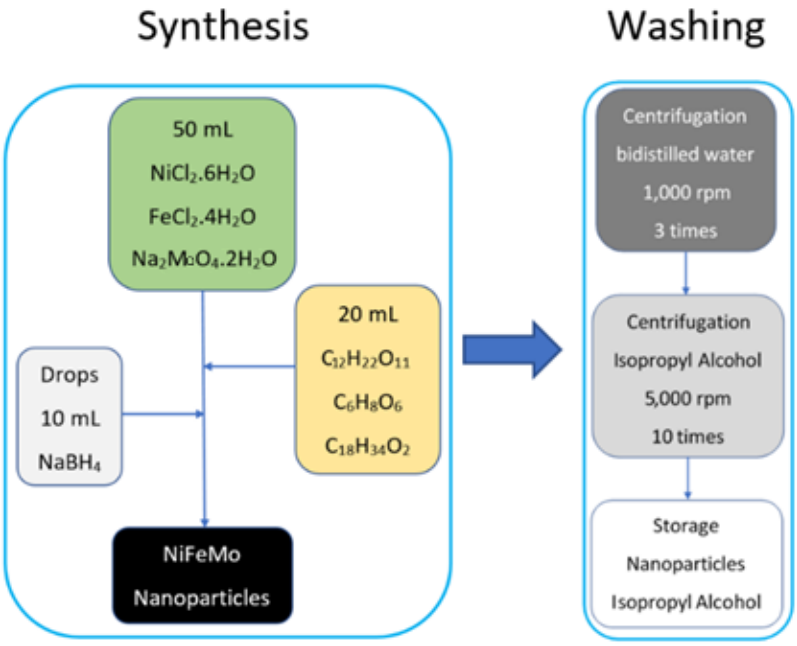

Fig. 1 Schematic representation of the synthesis and washing processes of NiFeMo nanoparticles.

operatingat 15 kV. The preparation of the sample for analysis in SEM/EDS consisted of drying in an oven at 60 °C and conditioning in the stub with double-sided carbon tape. The morphological analyses were performed in a TEM (Transmission Electron Microscopy) JEOL JEM 1200-EXII at 120 kV, as well as the microstructural analyses performed by SAED (Selected Area Electron Diffraction). The preparation of the sample was carried out by dripping 2 to 4 drops of the suspension of the nanoparticles in isopropyl alcohol in 200 mesh grids coated with a formvar/carbon film. For SAED analysis, an Au sample was used as a standard to calibrate the TEM camera constant. Structural analyses were carried out by XRD (X-Ray Diffraction) in a Bruker diffractometer model D8 Advanced using Cu kα radiation (λ = 0.15418 nm). The magnetic characterization was performed on a VSM (Vibrating Sample Magnetometer) from EG&G Princeton Applied Research model 4500 with a maximum magnetic field of 1.3 T. Measurements were performed at a temperature of 298 K. Before performing the measurements, the VSM was calibrated using a sample palladium standard provided by Quantum Design.

3. Results and Discussions

3.1 Morphological Analysis

The synthesized samples were analyzed by TEM, both the supernatant nanoparticles and the nanoparticles agglomerated in the lower part of the body. Fig. 2A shows that the supernatant nanoparticles are stabilized. The fit of a Gaussian curve to the size distribution histogram indicates average size of 36 nm with a width at half height of 30 nm FWHM (Full Width at Half Maximum), as shown in Fig. 2B. Fig. 2C shows the morphology of the nanoparticles in the form of aggregates. The magnification of this image is 10 times greater than that performed in Fig. 2A. With this level of detail, it is possible to observe small clusters.

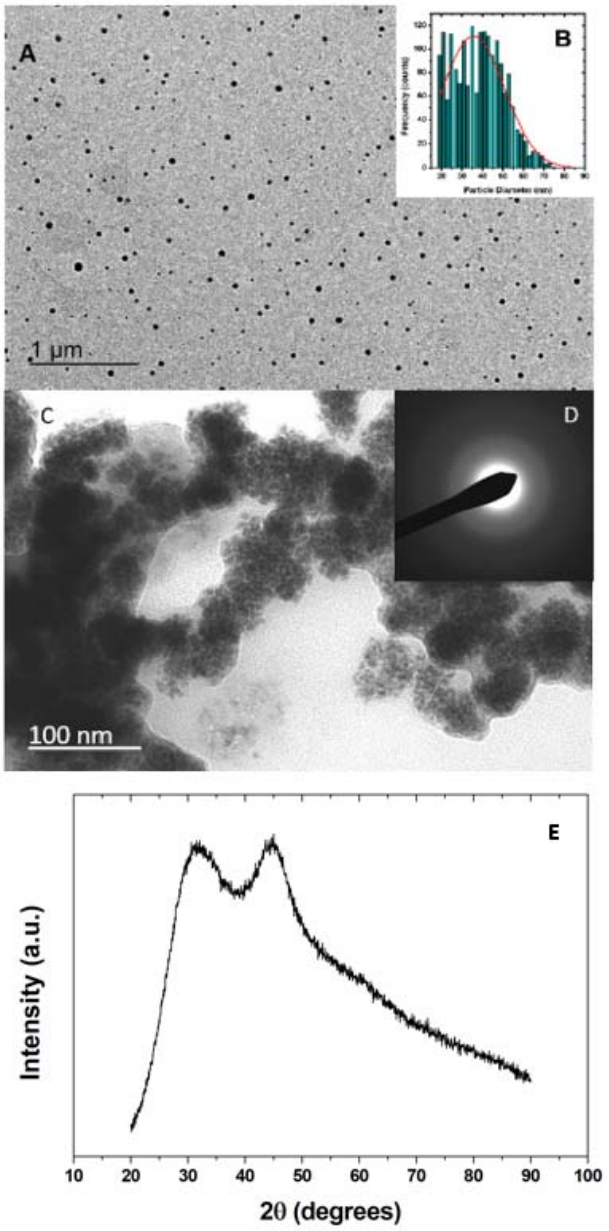

Fig. 2 TEM results for the nanoparticles as synthesized. (A) Image of the supernatant nanoparticles; (B) Size distribution from an image with magnification 2.5 times smaller than in the image in (A). The analysis was performed with 1,834 particles by the software Image J version 1.52; (C) Image of the precipitates extracted from the bottom body; (D) SAED of the particles of the image in (C); (E) Diffractogram of the nanoparticles presented in (C).

approximately spherical with about 40 nm, which in turn forms large clusters with no specific shape of the micron order. However, it is possible to observe that these small spherical clusters are formed by deformed

particles of variable size from 3 to 10 nm connected by a thin layer of 2 nm, which presents low contrast in the image. Fig. 2D shows the SAED results for the particles in Fig. 2C. The analysis of the SAED results indicates an amorphous structure without long-range crystalline ordering. The diffractogram shown in Fig.2E is in accordance with the qualitative analysis suggested by the SAED measure. The coherence length estimated by the well-known Scherer equation indicates a value of 0.55 nm, confirming the absence of long-range order.

These results suggest that very small particles from 3 to 10 nm are formed by the co-precipitation process, very similar to the results found by Wang et al. [12]. Subsequently form small spherical clusters approximately 40 nm on average and these also agglomerate producing micrometric particles without a specific shape. The analysis of the 2C image shows that the initial particles (3-10 nm) are connected by a layer of low electronic density, with a thickness of 3 nm on average, possibly a layer of the organic additives used in the synthesis.

3.2 Thermal Analysis

Due to the versatility of applications of NiFeMo nanoparticles, it would be interesting to investigate their thermal properties and determine the processes for releasing organic substances as a function of temperature. In this sense, TGA and DTGA measurements were performed. Fig. 3 shows the two curves. In the range of 22 to 150 °C, the DTGA curve shows a peak loss of mass at 91 °C. This peak in the DTGA curve is related to the loss of hydration water molecules (10% of the lost mass). The second temperature range of 150 to 360 °C with a peak of 306 °C is related to the combustion of organic additives with the release of CO_2 and H_2O, implying 6% of the lost mass. From 360 to 432 °C, a gain of 1% in mass is observed with the maximum gain indicated by the third peak in the DTGA curve at 397 °C. This mass gain can be attributed to an oxidation process of metallic nanoparticles. With the combustion of organic additives, sucrose and ascorbic acid produce ions $(OH)^-$. Associated with this supply of hydroxyl radicals in combination with the O_2 present in the atmosphere of the analysis, metal oxide-hydroxides (MeOOH) can be produced (considering Me = Ni, Fe), this being the cause of the mass gain. The enthalpy of formation of $Ni(OH)_2$ (ΔH = -538 kJ/mol) is more energetically favorable than NiOOH (ΔH = -394 kJ/mol). However, it must be considered that the supply of reagents may alter the products. In this case, the supply of OH^- radicals

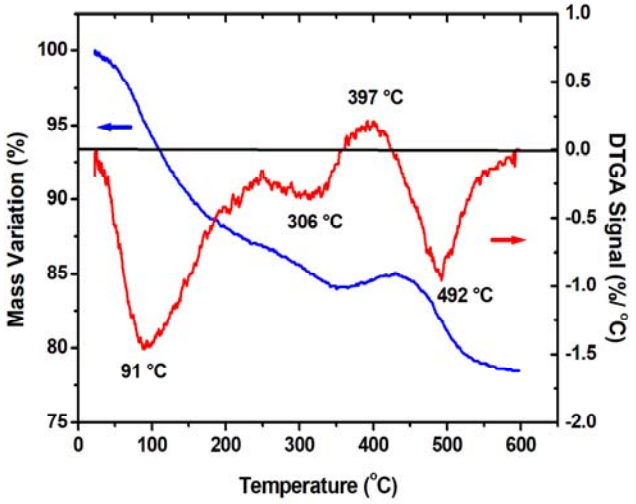

Fig. 3 Thermal analysis measurements. In blue, the mass variation curve, and in red, the mass loss derivative curve. The mass used in the analysis was 2.285 mg. The temperatures of the maximum mass variation rate (loss or gain) are shown in the figure.

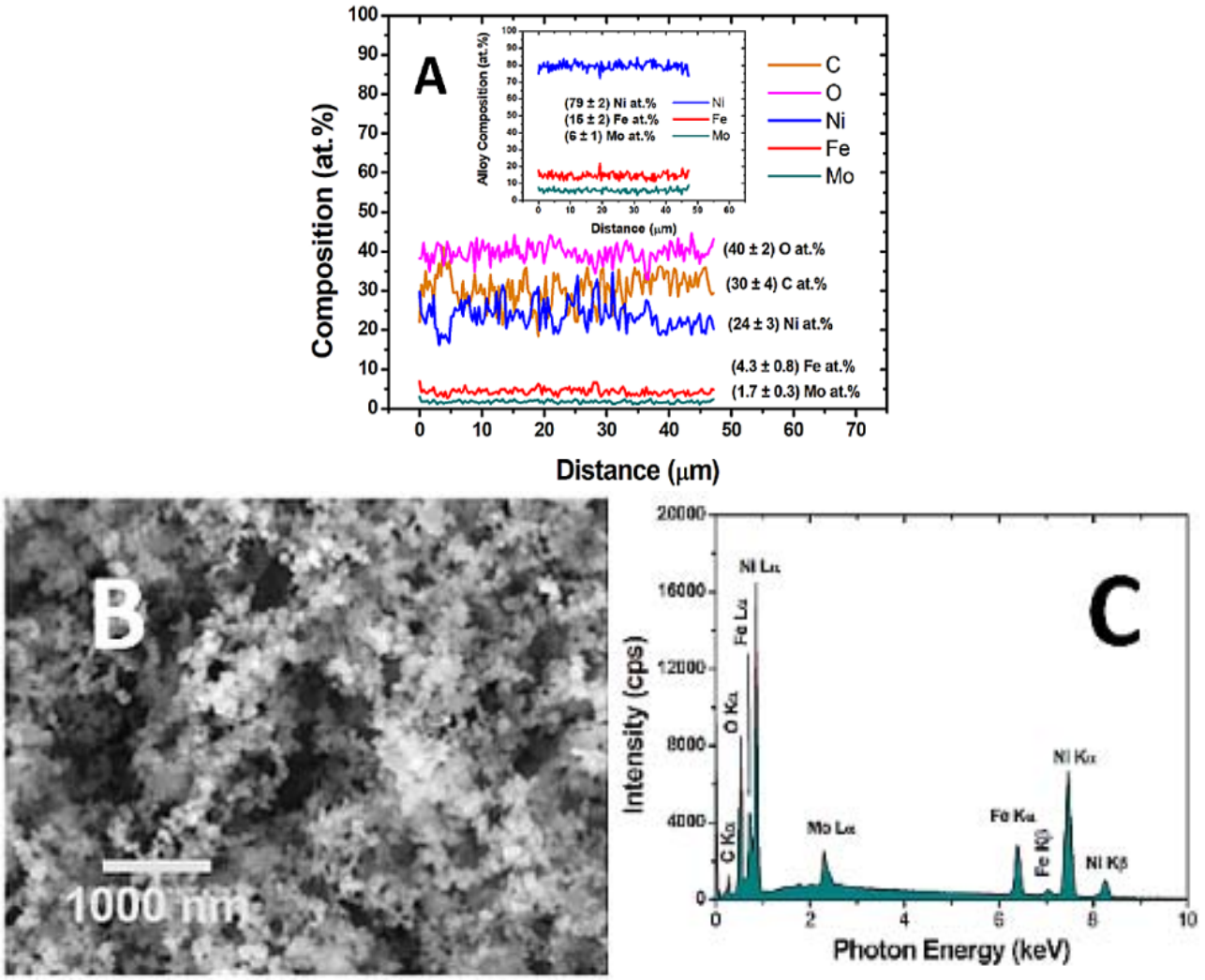

Fig. 4 Line profiles of 150 equal points above 50 µm. The points are separated by approximately 0.33 µm and the point size used was 17 nm with a voltage of 15 kV. This configuration of SEM and line profiles in the EDS control software guarantees measurement independence. In (A) composition profile of the synthesized nanoparticles the insertion is the normalized profiles for Ni, Fe, and Mo; (B) SEM image of the nanoparticles analyzed in (A); (C) EDS spectrum showing the elements detected at each point of the line profiles shown in (A).

is limited by the small molar fraction of ascorbic acid and sucrose present in the nanoparticles, while the supply of O_2 is widely offered in the test atmosphere by synthetic air. In the range of 432 to 600 °C, it is possible to observe a peak at 492 °C corresponding to 7% of loss of mass. This loss of mass is attributed to a process of decomposition of nanoparticles of the type (MeOOH) into (MeO) with the corresponding loss of H_2O produced in the process of decomposition of the oxides-hydroxides as well as the release of residues of CO and CO_2. Similar processes were observed in the production of NiO nanoparticles [18] and FeO [19].

3.3 Chemical Analysis

X-Ray Photon EDS (Energy Dispersion Spectroscopy) performed the elementary chemical analysis. The EDS results in Fig. 4A show that the synthesized nanoparticles have a high content of oxygen (40 ± 2) at.% and carbon (30 ± 2) at.%. These large percentages of O and C were already expected by the presence of organic additives in the synthesis of nanoparticles. Fig. 4B shows that the morphology of the samples prepared for the SEM/EDS analysis is very irregular, causing large fluctuations in the

quantitative analysis. Fig. 4C shows the EDS spectrum of one of the analyzed points, showing that only C and O are the non-constituent elements of the NiFeMo alloy. Renormalizing the data for only the elements Ni, Fe, and Mo, it is possible to determine the relative proportion of the alloy. The result of this analysis points to the following stoichiometry (79 ± 2) Ni at.%, (15 ± 2) Fe at.%, and (6 ± 1) Mo at.%. These results indicate that the stoichiometry of the alloy is very close to the desired $Ni_{79}Fe_{16}Mo_5$ (at.%).

3.4 Magnetic Analysis

The hysteresis curve of the nanoparticles is shown in Fig. 5. Note a typical curve of a soft ferromagnetic material, characterized by a low magnetization of the remnant (Mr) and with a small coercive field (Hc). However, the saturation magnetization value (Ms) is much lower than expected, which makes the relative contribution of Mr greater than desired. According to the work by Banerjee et al. [20] the expected value for the composition of the nanoparticles in this work should be 0.7 μ^B, however, the measured value indicates a lower order of magnitude. A possible explanation for this lies in the morphology and microstructure of the nanoparticles. The values presented by Banerjee et al. [20] are for massive crystalline samples produced by arc fusion from high purity powders. These samples are very crystalline and with large crystals. In the case of NiFeMo nanoparticles, they were synthesized by co-precipitation in the presence of organic additives. The microstructure presents a great structural disorder that, for SAED and XRD, the nanoparticles can be considered amorphous. Its morphology presents nanospheres with an average of 40 nm in diameter. TEM images revealed that these nanospheres have an internal morphology with even smaller particles with an average diameter of 5 nm spaced with thin layers of 2-3 nm of low contrast in the images. The compositional measures suggest that organic additives such as sucrose and ascorbic acid involve the smallest particles and act as binders for the formation of the 40 nm nanospheres. This morphology suggests that in addition to the structural disorder, which can reduce the value of Ms, a thin layer on the surface of the nanoparticles can react with the Fe atoms, having Fe^{3+} ions. Although the layer can be thin and superficial, the size of the 5 nm nanoparticles potentiates this surface effect in comparison with the volume effects. For this reason, these nanoparticles have a low Ms value.

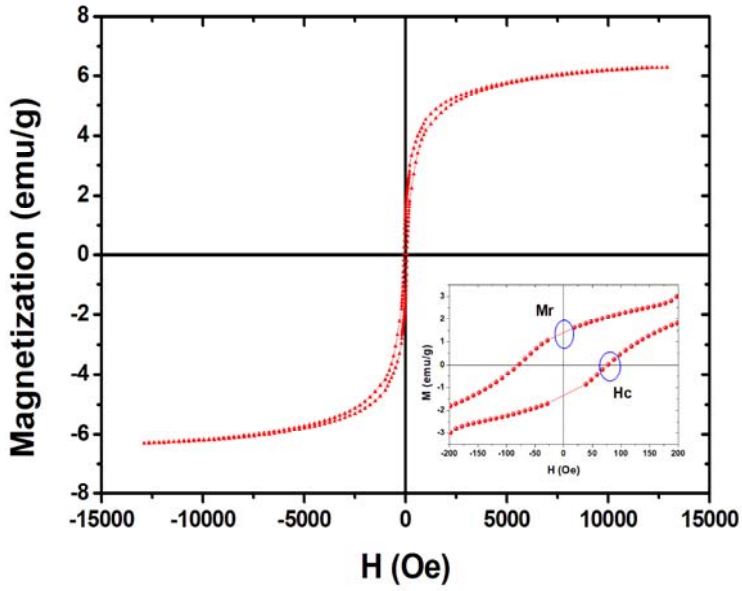

Fig. 5 Measurements of magnetization as a function of the magnetic field applied to the $Ni_{79}Fe_{15}Mo_6$ nanoparticles in the bottom body.

Table 1 Magnetic properties extracted from the hysteresis curve of the $Ni_{79}Fe_{15}Mo_6$ sample.

Ms (emu/g)	Mr (emu/g)	Hc (Oe)	Sample type	Ref.
6.28	1.41 22% Ms	77	NP (40 nm)	This work
-	45% Ms	0.03	Sintered micrometric powder	[21]
-	12% Ms	2.57	Sintered micrometric powder	[22]
-	Close to 0 out-of-plane	Close to 0 out-of-plane	Film of Nanospheres (140 nm)	[4]
-	96% Msin-plane	88 in-plane	Film of Nanospheres (140 nm)	[4]
-	-	20	Micrometric powder produced by ball milling (GS = 40 nm)	[6]
62.62	0.30 (0.5% Ms)	2.26	Micrometric powder produced by ball milling (GS = 40 nm)	[23]

In Table 1, we have some data on saturation magnetization, the remnant and coercive field magnetization for NiFeMo alloys with stoichiometries close to the nanoparticles studied in this work and with different production methods and, consequently, presenting different microstructures and morphologies. The value of Hc depends directly on the average value of the effective anisotropy constant and inversely with the value of Ms [24]. As previously discussed, the value of Ms for nanoparticles must be reduced, in a first approximation, by an order of magnitude. For this reason alone, a proportional increase of an order of magnitude in the value of Hc would be expected. Since the microstructure of the nanoparticles is amorphous and the nanoparticles are not linked as in the case of bulk samples or thin films, the effects caused by easy or hard magnetization axes would not be observed, as in the case of electrodeposited nanospheres film [4], which presents different values of Hc according to the direction of the applied magnetic field. Another aspect to be observed is that the effective anisotropy constant grows with d^6, where d is the particle size, for the situation where each particle is a single domain. When the microstructure is large enough to house multiple domains, the effective anisotropy constant decreases with d^{-1} [6]. This has been observed by Shen et al. [6] with increasing grain size and by Zhou et al. [4] with the increase in the thickness of the films. In the case of nanoparticles produced in this work, both the value of Ms and the value of the effective anisotropy constant, due to the particle size, contribute to the increase in Hc.

4. Conclusion

In summary, the results of the synthesis of stable nanoparticles of the magnetic alloy $Ni_{79}Fe_{15}Mo_6$ (at.%) produced by co-precipitation in the presence of organic additives were presented. The nanoparticles are formed into small amorphous nanoparticles with sizes from 3 to 10 nm coated with an encapsulation formed by the organic additives forming larger particles with an average size of 36 nm. Preliminary magnetic measurements relative to room temperature reveal the paramagnetic behavior of these nanoparticles with a remanence magnetization of 22% of the saturation magnetization as well as a low coercive field 77 Oe. These results are promising for possible technological applications both in the area of sensors and other electronic devices, but particularly in the area of human and animal health for the use of means for the development of diagnosis and therapy of numerous diseases that require less invasive treatment.

Acknowledgment

The authors thank the Brazilian agencies CNPq, CAPES, FINEP, and Fundação Araucária for their financial support. Thanks also go to the Electronic Microscopy Center at UFPR and the Multiuser Laboratory of the Department of Chemistry at UFPR for their services.

References

[1] Boothby, O. L., and Bozorth, R. M. 1947. "A New Magnetic Material of High Permeability." *Journal of Applied*

Physics 18: 173-6. https://doi.org/10.1063/1.1697599.

[2] Cowburn, R. P., Koltsov, D., Adeyeye, A. O., and Welland, M. E. 2000. "Lateral Interface Anisotropy in Nanomagnets." *Journal of Apllied Physics* 87: 7082-4. https://doi.org/10.1103/PhysRevLett.83.1042.

[3] Muñoz, A. G., Schiefer, C., and Kisker, E. 2008. "Anisotropic Permeability in Ultrasoft Electroplated NiFeMo/Cu Microwires: The Procopiu Effect." *Journal of Applied Physics* 103: 073904. https://doi.org/10.1063/1.2900883.

[4] Zhou, Q. G., Heard, P. J., and Schwarzacher, W. 2008. "Surface Roughness and Magnetic Properties of Electrodeposited NiFeMo Thin Films." *Journal of Applied Physics* 109: 054313. https://doi.org/10.1149/1.3050351.

[5] Chicinas, V. P., and Isnard, O. 2004. "Synthesis of the Supermalloy Powders by Mechanical Alloying." *Journal of Materials Science* 39: 5305-9. https://doi.org/10.1023/B:JMSC.0000039234.58490.78.

[6] Shen, Y. P., Hng, H. H., and Oh, J. T. 2004. "Synthesis and Characterization of High-Energy Ball Milled Ni-15%Fe-5%Mo." *Journal of Alloys and Compounds* 379: 266-71. https://doi.org/10.1016/j.jallcom.2004.02.032.

[7] Isnard, O., Pop, V., and Chicinas, I. 2005. "Magnetic and Structural Properties of the Supermalloy Powders Produced by Mechanical Alloying and Annealing." *Journal of Magnetism and Magnetic Materials* 290-1. 1535-1538. https://doi.org/10.1016/j.jmmm.2004.11.248.

[8] Popa, F., Isnard, O., Chicinas, I., and Pop, V. 2010. "Synthesis of Nanocrystalline Supermalloy Powders by Mechanical Alloying: A Thermomagnetic Analysis." *Journal of Magnetism and Magnetic Materials* 322: 1548-51. https://doi.org/10.1016/j.jmmm.2009.06.006.

[9] Neamtu, B. V., Geoffroy, O., Chicinas, I., and Isnard, O. 2012. "AC Magnetic Properties of the Soft Magnetic Composites Based on Supermalloy Nanocrystalline Powder Prepared by Mechanical Alloying." *Materials Science Engineering B* 177: 661-5. https://doi.org/10.1016/j.mseb.2012.03.029.

[10] Musaev, O. R., Midgley, A. E., Muthu, D. V. S., Wrobel, J. M., and Kruger, M. B. 2009. "X-Ray Diffraction of Permalloy Nanoparticles Fabricated by Laser Ablation in Water." *Materials Letters* 63: 893-5. https://doi.org/10.1016/j.matlet.2009.01.031.

[11] Liu, X. G., Or, Z. Q., Geng, D. Y., Han, Z., Wang, H., Li, B., Brück, E., and Zhang, Z. D. 2010. "Enhanced Absorption Bandwidth in Carbon-Coated Supermalloy FeNiMo Nanocapsules for a Thin Absorb Thickness." *Journal of Alloys and Coumpounds* 506: 826-30. https://doi.org/10.1016/j.jallcom.2010.07.085.

[12] Wang, H. L., Yan, J. M., Li, S. J., Zhang, X. W., and Jiang, Q. 2015. "Noble-Metal-Free NiFeMo Nanocatalyst for Hydrogen Generation from the Decomposition of Hydrous Hydrazine." *Journal of Materials Chemistry A* 3: 121-4. https://doi.org/10.1039/C4TA05360E.

[13] Mohamed El Shafey, A. 2020. "Green Synthesis of Metal and Metal Oxide Nanoparticles from Plant Leaf Extracts and Their Applications: A Review." *Green Processing and Synthesis* 9: 304-39. https://doi.org/10.1515/gps-2020-0031.

[14] Teeesukkasem, N., Chokradjaroen, C., Theeramunkong, S., Saito, N., and Watthanaphanit, A. 2019. "Synthesis of Au Nanoparticles in Natural Matrices by Liquid-Phase Plasma: Effects on Cytotoxic Activity against Normal and Cancer Cell Lines." *Applied Nano Materials* 2: 8051-62. https://doi.org/10.1021/acsanm.9b02106.

[15] Gorria, P., Fernández-Garcia, M. P., Sevilla, M., Blanco, J., and Fuertes, A. B. 2009. "Nickel Nanoparticles Deposited into an Activated Porous Carbon: Synthesis, Microstructure and Magnetic Properties." *Physica Status Solidi Rapid Research Letters* 1: 4-6. https://doi.org/10.1002/pssr.200802216.

[16] Alruqi, S. S., Al-Thabaiti, S. A., Malik, M. A., and Khan, Z. 2018. "Role of Surfactants: One Step Facile Synthesis of Hetero Structured Ag-Ni Alloy by Seed Less Approach." *Colloids and Surfaces A* 540: 36-47. https://doi.org/10.1016/j.colsurfa.2017.12.050.

[17] Hssaini, A., Belaiche, M., and Elansary, M. 2021. "One-Step Synthesis of Coated (Gd^{3+}, Er^{3+}) Co-doped Co-Ni Ferrite Nanoparticles; Structural and Magnetic Properties." *Journal of Materials Science-Materials in Electronics* 32: 11931-43. https://doi.org/10.1007/s10854-021-05823-8.

[18] El-Kemary, M., Nagy, N., and El-Mehasseb, I. 2013. "Nickel Oxide Nanoparticles: Synthesis and Spectral Studies of Interactions with Glucose." *Materials Science in Semiconductor Processing* 16: 1747-52. https://doi.org/10.1016/j.mssp.2013.05.018.

[19] Rudolph, M., Erler, J., and Peuker, U. A. 2012. "A TGA-FTIR Perspective of Fatty Acid Adsorbed on Magnetite Nanoparticles—Decomposition Steps and Magnetite Reduction." *Colloids and Surfaces A: Physicochem. Eng. Aspects* 397: 16-23. https://doi.org/10.1016/j.colsurfa.2012.01.020.

[20] Banerjee, M., Banerjee, R., Majumdar, A. K., Mookerjee, A., Sanyal, B., and Nigam, A. K. 2010. "Magnetism in NiFeMo Disordered Alloys: Experiment and Theory." *Physica B* 405: 4287-93. https://doi.org/10.1016/j.physb.2010.07.028.

[21] Ma, J. D., Qin, M. L., Wang, X., Zhang, L., Tian, L. S., Zhang, X. F., Li, X. Q., and Qu, X. H. 2014. "Microstructure and Magnetic Properties of Fe-79%Ni-4%Mo Alloy Fabricated by Metal Injection Molding." *Powder Technology* 253: 158-62. https://doi.org/10.1016/j.powtec.2013.11.011.

[22] Neamtu, B. V., Chicinas, I., Isnard, O., Ciascai, I., Popa,

F., and Marinca, T. F. 2014. "Consolidation and DC Magnetic Properties of Nanocrystalline Supermalloy/Iron Composite Cores Prepared by Spark Plasma Sintering." *Journal of Magnetism and Magnetic Materials* 353: 6-10. https://doi.org/10.1016/j.jmmm.2013.10.021.

[23] Ghosh, N. C., Das, H. N., Gafur, M. A., and Akther Hossain, A. K. M. 2015. "Investigation of Structural and Magnetic Properties of Ni-Fe-Mo Nanocrystalline Alloy Synthesized by Mechanical Alloying." *Journal of Engineering Science* 6: 105-10.

[24] Suzuki, K., and Cadogan, J. M. 1998. "Random Magnetocrystalline Anisotropy in Two-Phase Nanocrystalline Systems." *Physical Review B* 58: 2730-9. https://doi.org/10.1103/PhysRevB.58.2730.